



HAL
open science

From the thermodynamics of constitutive laws to the thermomechanical experimental characterization of a semicrystalline polymer from IR imaging

Stéphane André, Norbert Renault, Yves Meshaka, Christian Cunat

► To cite this version:

Stéphane André, Norbert Renault, Yves Meshaka, Christian Cunat. From the thermodynamics of constitutive laws to the thermomechanical experimental characterization of a semicrystalline polymer from IR imaging. *Continuum Mechanics and Thermodynamics*, 2011, 24, pp.1-20. 10.1007/s00161-011-0205-x . hal-01462877

HAL Id: hal-01462877

<https://hal.science/hal-01462877>

Submitted on 9 Feb 2017

HAL is a multi-disciplinary open access archive for the deposit and dissemination of scientific research documents, whether they are published or not. The documents may come from teaching and research institutions in France or abroad, or from public or private research centers.

L'archive ouverte pluridisciplinaire **HAL**, est destinée au dépôt et à la diffusion de documents scientifiques de niveau recherche, publiés ou non, émanant des établissements d'enseignement et de recherche français ou étrangers, des laboratoires publics ou privés.

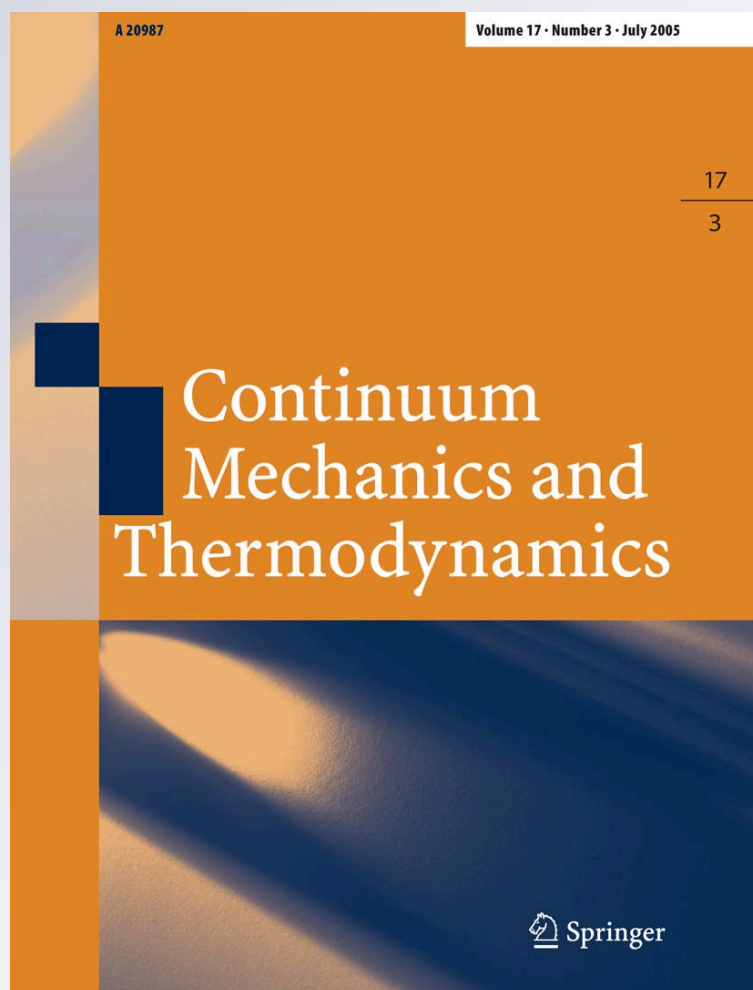
From the thermodynamics of constitutive laws to the thermomechanical experimental characterization of a semicrystalline polymer from IR imaging

Stéphane André, Norbert Renault, Yves Meshaka & Christian Cunat

**Continuum Mechanics and
Thermodynamics**

ISSN 0935-1175

Continuum Mech. Thermodyn.
DOI 10.1007/s00161-011-0205-x



 Springer

Your article is protected by copyright and all rights are held exclusively by Springer-Verlag. This e-offprint is for personal use only and shall not be self-archived in electronic repositories. If you wish to self-archive your work, please use the accepted author's version for posting to your own website or your institution's repository. You may further deposit the accepted author's version on a funder's repository at a funder's request, provided it is not made publicly available until 12 months after publication.

Stéphane André · Norbert Renault · Yves Meshaka ·
Christian Cunat

From the thermodynamics of constitutive laws to the thermomechanical experimental characterization of a semicrystalline polymer from IR imaging

Received: 22 November 2010 / Accepted: 21 September 2011
© Springer-Verlag 2011

Abstract This paper aims at presenting the complete metrological problem associated to the thermomechanical characterization of materials. With this purpose in view, we first present a model based on irreversible thermodynamics that allows straightforward formulation of the set of the required state laws. Then, the state law, which links both entropy and temperature variables, is used within an entropy balance. It leads to the heat equation allowing for the identification of the different contributions involved in the apparent Thermomechanical Heat Source (THS). This THS is measured during the tensile experiment of a semicrystalline polymer, thanks to the monitoring of in-situ infrared temperature fields and the subsequent application of numerical reconstruction algorithms. Both stress-strain and THS-strain curves obtained experimentally over the same representative elementary volume are used simultaneously to identify the parameters of the behavioral model. The results first show that the model is able to describe the measured THS. Secondly, they allow for a clear analysis of various thermomechanical contributions (thermoelastic effect, total pure intrinsic dissipation, entropic couplings contribution reflecting microstructure transformations), which can be very helpful in understanding microscopic deformation phenomena.

Keywords Thermomechanics · Irreversible thermodynamics · Quantitative thermography · Constitutive behavior · Plasticity

Communicated by Andreas Öchsner.

S. André (✉) · C. Cunat
LEMTA, Nancy-University, CNRS UMR7563,
2 Avenue de la Forêt de Haye, B.P. 160, 54504 Vandoeuvre-lès-Nancy, France
E-mail: Stephane.Andre@ensem.inpl-nancy.fr
Tel.: +33-383-595730
Fax: +33-383-595551

C. Cunat
E-mail: Christian.Cunat@ensem.inpl-nancy.fr

N. Renault
L2MGC, Université de Cergy-Pontoise, Site de Neuville, UFR sciences et techniques,
5 Mail Gay-Lussac, 95011 Neuville-sur-Oise, France
E-mail: norbert.renault@u-cergy.fr

Y. Meshaka
IJL, Nancy-University, CNRS UMR7198,
Ecole des Mines de Nancy Parc de Saurupt, CS 14234, 54042 Nancy Cedex, France
E-mail: yves.meshaka@eigm.inpl-nancy.fr

1 Introduction

Since their irruption in the industry, polymers have supplanted metallic materials in many mechanical applications, with more and more highly technical specifications. The objective of getting more efficient constitutive laws in solid rheology has led researchers in the last decades to focus on the thermomechanical couplings occurring unavoidably in the matter. This means first that constitutive laws must be based on the thermodynamics of irreversible processes framework and secondly that experimental tools must be developed to analyze the heating effects accompanying the mechanical solicitations of materials. In this latter domain, one can obviously note that many efforts are still to carry on. The main goal is generally to identify the percentage of mechanical energy added to a sample that appears as heat, the remaining being “stored” in the microstructure (also named “cold” work). Such a preoccupation is very old that could be traced back to early works done on metals [20,56]. The interested reader may consult the review of Bever [7] for all the activities conducted up to the 1970s. Characterizations of that partition between mechanical and thermal energies can be reached according to two strategies. Measuring heat fluxes in home-made deformation calorimeters [1,50] has the advantage of giving a direct access to the thermal power at stake but gives a global information at a scale that is much larger than the representative elementary volume (REV) assumed for thermodynamical state laws. Measuring temperatures [54,55] has the advantage of giving a more local information but does not reflect any intrinsic thermomechanical behavior of the matter as it depends on entropy exchanges with the REV surroundings (heat conduction, convection, and possibly radiation). Therefore, a model is necessary to convert this data and to produce the desired experimental information: the heat power dissipated or absorbed by the matter as a function of space and time. The above references relate to polymer materials but of course, following the routes opened by the initial studies [20,56], most of the papers presenting experimental and/or theoretical results in this field relates to the behavior of metals. For these materials indeed, thermomechanical couplings are investigated through different phenomena such like the detection of fatigue limit, crack propagation, or more generally damaging phenomena, the forming and machining processes where the interaction between the tool and the material piece is concerned, high strain (dynamical) tests like in the Kolsky bar test. Each of these topics is quasi a scientific field per se with proper specificities and approaches. They offer in most cases the great advantage of avoiding to solve the inverse heat conduction problem (IHCP) in order to reconstruct the thermomechanical heat sources (THS) because most of the approximated solutions are valid and give a direct access to them. For example, the hypothesis of adiabaticity can be undoubtedly used in the case of dynamical test as shown in the study of [28]. Fatigue studies deal with cyclic solicitations and therefore authorize a “lock-in” analysis like for example in the works of [29]. They also diminish the metrological difficulties in the sense that a more elevated energy is involved by cumulative effect that enhances the magnitude of the recorded signals. Very few studies try to calculate the heat source terms from approximated solution of the heat transfer equation in the case of quasi-static tests [11,12] or in the case of thermal effects associated to cyclic loadings [19] and further less to reconstruct this term with a real inverse procedure [47,59]. This latter becomes nowadays essential since the widespread recourse of InfraRed (IR) cameras with detector arrays that allows good spatial and sensitivity resolution as well as non-intrusive temperature measurements.

Regarding theoretical works, numerous papers deal with the development of appropriate thermomechanical models, but rely on different versions or lectures of the thermodynamics of irreversible processes (TIP). In this field, there are different schools of thought that will not be discussed here. The reader can refer to basic articles or textbooks in this field like among others those of [13,32,37]. Papers [2,30,51] give examples of the comparison between experimental thermal behavior of elastoviscoplastic materials and the predicted results issued from thermodynamical models.

The goal of this paper is to present a fully consistent thermodynamical framework and associated inverse methodology applied to experimental thermomechanical observables. Those are obtained at the representative elementary volume (REV) scale during quasi-static tension of a polymer material. The experimental platform we used is described first in Sect. 2. Its main features are part of the originality of our works. The originality lies secondly in the thermodynamical framework presented in Sect. 3, which departs from classical approaches based more or less on ad-hoc internal variables [32]. The Callen/Tisza axiomatic for establishing state laws [10,58] is followed here, which do not invoke any 1st principle to derive the heat equation. Use is also made of mechanochemistry concepts [24] to describe internal mechanisms of deformation in order to take full advantage of De Donder approach of irreversibility in non-equilibrium systems [17,18]. With this model, a real inversion of the heat equation can be performed in order to estimate the THS. Two different inverse methods are used [48,49], which differs from other methods (e.g., those of [12]). We show in this paper that they produce the same results, which constitutes a guarantee with respect to the results we got. It will be the aim of Sect. 4 to

deliver and discuss the results obtained from experimentally recorded thermographic films obtained during uniaxial cold drawing of a semi-crystalline polymer (SCP). Finally, in Sect. 5, the complete methodological loop relative to the thermomechanical characterization of materials will be closed. The thermodynamical constitutive laws can be confronted to both thermomechanical and mechanical observables to check their potential relevancy. This will be made through identification of the model parameters. Some conclusions will be drawn regarding the physical aim of such type of studies: the understanding of the basic thermal phenomena occurring during the deformation path as potentially useful signatures of complex internal micromechanisms.

2 Experimental setup

An experimental platform has been developed around a classical tensile testing machine (servo-hydraulic MTS 810 load frame). It is based on three coupled (and compatible) optical techniques that allow for the measurement of three different kinds of observables on the same REV of a polyethylene specimen [4].

- The first component monitors the engineering macroscopic variables that are the stress and corresponding strain. It is based on a video-extensometer (VIDEOTRACTION[®]). This technique [21] relies on the videomonitoring of markers previously inscribed on the specimen on its front face (Fig. 1a, b). It allows for a ‘live’ measurement of the true strains ε_y and ε_x according to the frame axis given in Fig. 1c. Hencky definitions are considered for these true uniaxial strains. They are calculated according to $\varepsilon = \ln(l(t)/l_0)$ where l_0 and $l(t)$ are the measures of distances between the barycenters of two given markers at the initial and current stages of the deformation process. Seven markers are plotted in the form of a cross in the central part of the specimen, with minimum width (Fig. 1b, c). This ensures the necking and thus the maximum strains to develop in a well-defined zone considered as a REV for the thermomechanical analysis made in Sect. 5. The image analysis consists in a simple identification of the markers through binarization, computation of the barycenters of the spots, interpolation between the 5 longitudinal markers to obtain the current true strain $\varepsilon_y^{\text{REV}}$ at the exact location of the REV (Plot of Fig. 1c). The CCD camera (I2S, with a resolution of 575×560 px) is mounted on the top of a telescopic drive to follow the movement of the observed zone. A software program carries out the data acquisition, the image analysis in real time and the command of both the MTS machine and the telescopic drive. Recent measurements using digital image correlation (ARAMIS 3D system from GOM Instruments) show that the longitudinal strain as measured by Videotraction lies within an error of less than 4% (accounting for both the 2D plane measurement, and the necking phenomenon that do not conserve the principal axis reference frame).

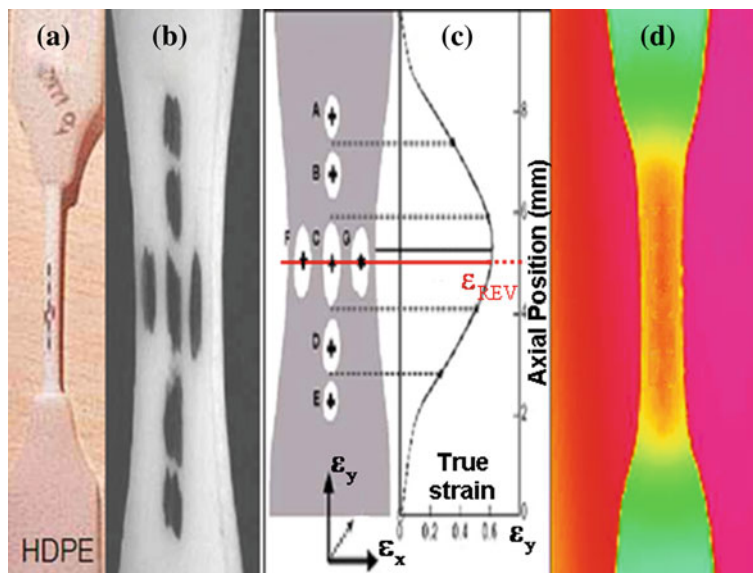


Fig. 1 Videoextensometer system and infrared imaging: **a** deformed specimen, **b** snapshot of videotraction markers, **c** principle of videotraction longitudinal strain measurement on a REV, **d** temperature field for a given deformation with necking

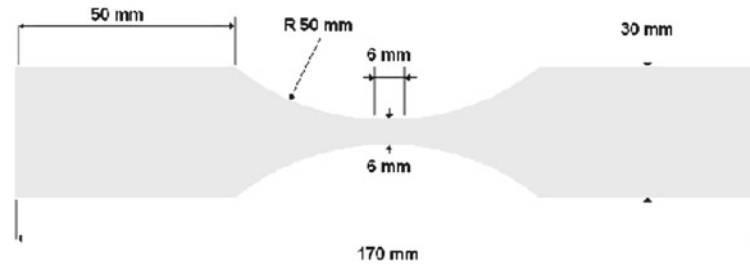


Fig. 2 Shape and dimensions of the specimen used for tensile test

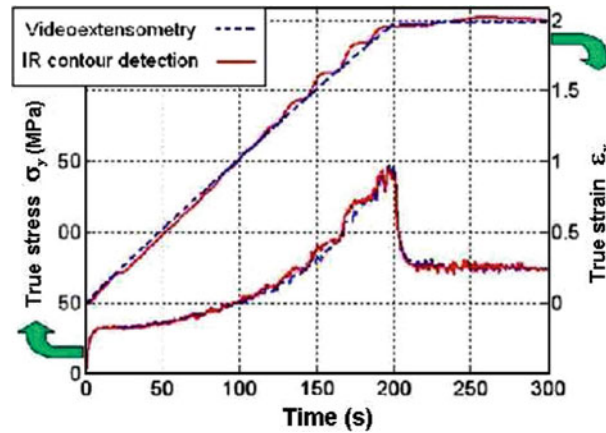


Fig. 3 Stress-Strain curve and longitudinal strain as produced by videoextensometry or IR contour detection

The force cell signal enables the computation of the true stress by the formula $\sigma = F/S = F/S_0 \exp(-\varepsilon_x - \varepsilon_z) = F/S_0 \exp(-2\varepsilon_x)$ as it has been checked that with an initial -nearly- square section, we always have $\varepsilon_x = \varepsilon_z$ during the test. The advantages of this technique are: (1) it allows for a control of the machine either in stress or strain or strain rate as the image processing is fast compared to full-field optical measurements, (2) it is a light, flexible technique that can be used in combination with others and (3) the results do not depend on the geometrical shape of the specimen that is given in Fig. 2. Figure 3 shows the typical results obtained for the true stress-true strain behavior of a high density polyEthylene (HDPE) specimen for a given deformation rate.

- The second component has been introduced to account for the thermomechanical couplings phenomena. An infrared imager (CEDIP JadeIII—NEDT 20 mK) observes the temperature field at the back surface of the specimen (opposite face to the markers—Fig. 1d). This camera is also mounted on a telescopic drive enslaved to the first one (precision of 2 mm for a travel distance of 100 mm) in order to ensure that the IR images remains centered on the REV during the whole test. From these thermographic images, the reconstruction process described in Sect. 4 will allow for heat source recovery over the whole specimen. From this, the THS versus strain curves at the REV location—and hence at the same location where the stress-strain curve is measured—can be plotted and used as observable signal for thermomechanical investigation of the material behavior. Besides this key objective, a contour detection has been implemented on the thermal images in order to measure the transverse deformation in the center of the specimen. Although this signal appears noisy, it is interesting to note on Fig. 3 that assuming a constant Poisson coefficient of 0.49 confirms the measurement given for the longitudinal strain by Videotraction. No special coating is required on the specimen surface for IR measurements because the emissivity of our natural HDPE is close to 1. A spray of black paint is yet applied in practice in order to produce a more homogeneous emissivity distribution. Temperature maps obtained with and without such coating give the same results except that the noise is diminished, which is important in view of data inversion.
- A third component was added to the above two, which is based on the common observation that most of the semi-crystalline polymers, initially turbid and milky in non-deformed state, turns strongly white under loading. This is the result of microstructural mechanisms (plasticity and damaging) that could be correlated to thermal signatures. A new technique based on the diffusion transport of incoherent light in

turbid media has been implemented on the platform. It provides in-situ quantitative characterization of the microstructure evolutions. It is not the aim of the present paper to describe this technique and the results it has brought. It is mentioned here as it has confirmed the different regimes of deformation (or damaging) processes as revealed by the present thermomechanical analysis which, in a certain sense, validates the results presented in this paper. The reader may refer to [5] in order to go in deep details with this matter.

The three techniques can work simultaneously. The shape and dimensions of the specimen we used are given in Fig. 2. They were optimized in order to produce intrinsic measurements (independent of the geometry). The thickness of the specimen is 4 mm. The HDPE material used for the present works is Grade “500 Natural” produced by Röchling Engineering Plastics KG. The molecular weight and density are, respectively, of 500,000 g/mol and 0.935 g/cm³. Differential scanning calorimetry gave a crystallinity index of 68 wt%.

3 Inversion algorithms

Many studies can be found in the literature that deal with the problem of heat source reconstruction as those reported for example in [22,33,47,52]. But due to the great variety of the physical problems at hands, the specific constraints they bring, and also to the different ways that exist to formulate the inverse problem, very different methods have been used. As a consequence, no standard tool is still available. It is then necessary to state first the requirements and objectives of the inversion algorithms we developed.

3.1 Assumptions and basic features of the algorithms

Applying a reconstruction algorithm to the thermographic film acquired during a mechanical test imposes to consider at least four basic facts:

- The first one issues from the variety of coupling phenomena that induces thermal effects having different magnitudes. In our experiments made on a SCP and under quasi-static tests, the temperature variation can be due to thermoelasticity in an amount of 0.5 K or to localized heating phenomena where the temperature rise can be as large as 20–30 K, depending on the strain rate. The reconstruction algorithm must be very precise in order to be discriminating with respect to this.
- One must obviously consider also that the heat sources are not necessarily homogeneous in space for two reasons: first, the shape of the specimen induces a structure effect (the stress and strain fields are not homogeneous in space) and second, some localization phenomena are generally expected (necking, shear bands propagation, cracks initiation). Therefore, and as second feature, the algorithms must meet an accurate spatial resolution.
- As already mentioned, the algorithms will be devoted to applications in conditions of quasi-static tests. Small enough deformation rates are considered so that no noticeable advection effect is expected to occur. The range of Peclet numbers reached in the experiments is of the order of 1 as a maximum. In the literature, similar experiments are made with an infrared camera that is fixed with respect to the load frame. In this situation, advective aspects of the heat transfer are maximum. In our case, due to the movement of the infrared camera that is enslaved to the videoextensometer, a perfect symmetry is observed with respect to the REV Center. Advection effects are therefore limited, and our efforts have been concentrated on the solution of the IHCP with a governing heat equation having parabolic structure.
- The fourth and final feature of the algorithms is that they have been developed in order to be independent of the real boundary conditions applied to the specimen in the observed plane (especially in the grips) and also of the frame of the image. One may indeed wish to observe a limited area of the specimen. Therefore, the algorithm has been developed with the essential concern of using the temperature measured at the edges of the image (fully included in the specimen) as boundary conditions of the thermal problem. This induces more flexibility for the operator (no assessment of the type of boundary conditions) and allows for the development of a more versatile computation code. Concerning the boundary conditions, for the out-of-plane directions (front and back surface of the specimen), a fin approximation has been considered (which explains the 2D or 1D character of the reconstruction algorithm) with a global heat exchange coefficient representing the effect of convection due to the surrounding air and to the linearized radiative heat loss.

In addition to these four features, the inverse algorithm requires to consider regularization techniques in order to stamp out the ill-posed character of such archetypal inverse problem. The Laplacian-diffusion operator

works indeed like a low-pass smoothing filter (with respect to high fluctuations). Therefore, it can hardly go back to the original highly resolved distribution of some initial perturbation from information obtained at later elapsed times, and all the less in the presence of noise on the measured input information.

3.2 Physical model used for inversion

The 2D parabolic heat equation just evoked is always stated from the first law of thermodynamics. But in thermodynamics of irreversible processes, it can be more simply derived from the entropy balance of a REV (the cornerstone of the theory of TIP according to A. Münster [40]). In terms of specific quantities (extensive quantities scaled in all equations below by the total volume), this latter can be written classically [32,40]:

$$\dot{s} = \dot{s}_e + \dot{s}_i \quad (1)$$

The entropy rate exchanged with the REV environment corresponds to:

$$\dot{s}_e = -\nabla \cdot \left(\frac{J_q}{T} \right) = -\frac{\nabla \cdot J_q}{T} + \frac{J_q}{T^2} \cdot \nabla T \quad (2)$$

assuming no convective transport of entropy. The entropy rate source (null at equilibrium) is composed of a relaxation part (irreversible dissipation noted \mathcal{D}) and a transport part (due to the non-uniformity of the intensive parameters) [40]. This leads to:

$$\dot{s}_i = \dot{s}_i^{\text{relaxation}} + \dot{s}_i^{\text{transport}} = \frac{\mathcal{D}}{T} - \frac{J_q}{T^2} \cdot \nabla T \quad (3)$$

Providing that Fourier's law is considered for the heat flux J_q (λ : thermal conductivity), one thus get

$$\dot{s} = \frac{\lambda \Delta T}{T} + \frac{\mathcal{D}}{T} \quad (4)$$

for the entropy balance.

The next (and second) step of the model requires to write the state evolution equation of the entropy, following the route of many classical authors [10,18,46]. Shortly described, it consists first in assuming the validity of the Euler fundamental equation (in energy representation), even in systems out of equilibrium [10].

$$u(s, \underline{\underline{\varepsilon}}, z^j) = Ts + \underline{\underline{\sigma}} : \underline{\underline{\varepsilon}} + \sum_k \mu_k n_k \quad (5)$$

The internal energy depends on the independent extensive quantities that are: the entropy S (introducing the thermal component of the internal energy), volume V (mechanical component), and number of moles of chemical species N_k (chemical component). It is written in (5) in specific form (divided by the volume of the REV) according to the Euler homogeneity property of first degree. The tensorial notation used here to denote the stress and strain tensors in a generalized picture is abandoned from now on for clarity and because uniaxial application is considered.

The third step follows the initial suggestion of [17], and many other authors [18,46] who consider that relaxation phenomena are due to irreversible processes that are nothing else but internal reorganizations. This 'chemical' viewpoint has been later adopted in solid rheology (see the book of [32], Chapter 7) but has been, above all, legitimated by numerous works in the field of Mechanochemistry [24,31,42]. The chemical energy is expressed in terms of variables (A Affinity, z extent of advancement of processes j) instead of variables (μ chemical potential, N mole numbers of chemical components k or n_k in specific form). This is a consequence of what can be considered as a scale transition made through equation:

$$\sum_k \mu_k n_k = \sum_k \mu_k \left\{ \sum_j v_k^j z^j \right\} = - \sum_j A^j z^j \quad (6)$$

where De Donder affinity is defined by $A^j = - \sum_k \mu_k v_k^j$. It has the status of a real state function [46] and can be defined in terms of first partial derivative of thermodynamic potentials as, for example, $A = -u_{,z} |_{(S,V,\varepsilon)}$.

Coefficient v_k^j is the stoichiometric coefficient associated to the reaction j in which specie k is involved. The extent of advancement z can be regarded in a plastic phenomenon as the number of elementary motions concurring to create a propagation front (dislocation lines progress through redistribution of atomic bonds). Of course, and following the viewpoint of [40], microstructural evolution in the solid state rarely correspond to well-defined stoichiometries when mechanical deformation is under concern. Such complexity is treated in the book of Gutman [24], especially chapter 3 dedicated to irreversible interaction of processes of chemical reaction, plastic deformation, and dispersion of solids. In the book of Nowick and Berry [42] also, chapter 5 fully describes the connection between mechanical models, internal variables and the thermodynamic basis for relaxation spectra, following early works of Staverman and Schwartzl [53] and Meixner [39]. Ad-hoc defined internal variables introduced without implicit references to mechanisms of pure chemical origin are also used in the thermodynamic framework of TIPIV (thermodynamics of irreversible processes with internal variables) as in the works of Maugin and Muschik [38,41]. They require the introduction of an additional dissipation pseudopotential to complies with the TIP structure. The ‘hidden’ character of these variables is also fully accepted by the promoters of such approaches who still use the notation A and wording ‘Affinity’ to qualify the ‘non-equilibrium’ forces, recognizing that way the contribution of chemists to thermodynamical foundation of a theory of irreversibility. Although the formulations can converge in their mathematical structure and ability to capture the behavior of elasto-visco-plasticity of deformable materials, they are conceptually different as the ingredient of invoking the chemical thermodynamics of De Donder, De Groot and Mazur, Prigogine offers alternatives to model the kinetics of the relaxation processes, especially through statistical mechanics.

We can turn our attention to the fourth step of the model. Following Euler equation and the formalism of [10,58], the thermodynamic equations of state for evolutionary problems in thermomechanics are written

$$\dot{T} = \dot{T}(s, \varepsilon, z^j, \dot{s}, \dot{\varepsilon}, \dot{z}^j) \quad (7a)$$

$$\dot{\sigma} = \dot{\sigma}(s, \varepsilon, z^j, \dot{s}, \dot{\varepsilon}, \dot{z}^j) \quad (7b)$$

$$-\dot{A}^j = -\dot{A}^j(s, \varepsilon, z^j, \dot{s}, \dot{\varepsilon}, \dot{z}^j) \quad (7c)$$

which leads to the matrix formulation:

$$\begin{pmatrix} \dot{\beta} \\ -\dot{A} \end{pmatrix} = \begin{pmatrix} a^u(\boldsymbol{\gamma}, z) & \mathbf{b}(\boldsymbol{\gamma}, z) \\ {}^t\mathbf{b}(\boldsymbol{\gamma}, z) & \mathbf{g}(\boldsymbol{\gamma}, z) \end{pmatrix} \begin{pmatrix} \dot{\boldsymbol{\gamma}} \\ \dot{\mathbf{z}} \end{pmatrix} \quad (8)$$

A clear separation is made between observable state variables ($\beta, \boldsymbol{\gamma}$) and unobservable dissipative variables ($-A, \mathbf{z}$). In this formulation, matrix a^u is the *unrelaxed* (instantaneous) stability matrix in Tisza’s generalized approach of classical thermodynamics. Considering an uniaxial cold-drawing test, with deformation and temperature rates as control variables (vector $\boldsymbol{\gamma} = (T, \varepsilon)$), the Helmholtz free energy $f(T, \varepsilon, z) = u - Ts$ shall be considered rather than the internal energy $u(s, \varepsilon, z)$. Thanks to Legendre transformations, the (dual) ‘response’ vector $\dot{\beta}$ corresponds to $(-\dot{s}, \dot{\sigma})$. Such writing gives direct access to the calculations of affinities A^j as function of the other state variables (T, ε, z^j) and especially to the heat resulting from intrinsic dissipation obtained according to $\mathcal{D} = \dot{A}^j \dot{z}^j$. Focusing on the generic first line of (8), the state equation for the entropy rate is simply:

$$-\dot{s} = \left(-\frac{\rho C_u}{T} \dot{T} - \alpha_u E_u \dot{\varepsilon} \right) + \mathbf{b}_{sz} \dot{\mathbf{z}} \quad (9)$$

and is made of three terms. The first term corresponds to the instantaneous or unrelaxed natural dependence between (s, T) , where $\rho C_u/T$ is the corresponding stability coefficient of matrix a^u . The second term of the right-hand side corresponds also to an instantaneous or *unrelaxed* coupling term but now between observable variables (s, ε) . This term represents the well-known thermoelastic effect and involves the dilatometric coefficient α_u , E_u being the instantaneous Young modulus for the uniaxial test. The last term corresponds to the coupling between variables (s, z^j) , i.e., describes the inelastic (or dissipative or delayed) component to the entropy evolution due to relaxation phenomena. In this approach [15,16], it has been shown that it can be advantageously replaced according to the following equation:

$$\dot{s}^{\text{inelastic}} = \mathbf{b}_{sz} \dot{\mathbf{z}} = - \sum_j \frac{b^j(\boldsymbol{\gamma})(z^j - z^{j,r})}{\tau_z^j} = - \sum_j \frac{(s^j) - (s^{j,r})}{\tau_s^j} \quad (10)$$

This equation is a key one in the description of the kinematics of irreversible processes through a set of first order differential equations. Except for the last equality, which is not written in general, the first part of this

relation is common to different approaches of continuum TIPVI dealing with relaxation behaviors (Eq. 4.25 in [38]). It introduces the concept of a relaxed state and of an operator of distributed relaxation times.

Relaxed state: This state has been characterized very clearly by Prigogine ([46], Tome II, Part 5: Transformations et déplacements d'équilibre) as the stationary state corresponding to a null affinity rate, which means constant affinity $\dot{A}^r(\dot{\gamma}, \dot{z}^r) = 0$. This state was referred to as 'isoaffin state' by Prigogine but the term 'relaxed' due to DeGroot and Mazur [18] is preferred here. In this state and in the picture of Gurtin [23], microforces working for equilibrium recovery are constant. This state must not be confused with the equilibrium situation classically defined by $A^{\text{eq}} = 0$. In other TIP approaches, the recourse to special out-of-equilibrium states of the system is also addressed, as the result of some projection, which associated points of non-equilibrium state space with points of equilibrium state space (e.g., the Local Accompanying State [38]). In (10), relaxation is made from the current state to a relaxed one (explaining the use of s^r to denote the entropy in the relaxed state), according to an operator of distributed relaxation times indexed by upperscript j . The relaxed state has to be modeled in the approach. The most simple way to do this is to introduce a relaxed thermodynamic coefficient \mathbf{a}^r and to write a linear relationship in the form $\boldsymbol{\beta}^r = \mathbf{a}^r \boldsymbol{\gamma}$. It can be demonstrated that \mathbf{a}^r can depend on the history of the material in an irreversible way. For the (entropy and temperature) state equation, it will lead to a modeling of the form $s^r = \frac{\rho C_r}{T} \dot{T}$.

Operator of distributed relaxation times: τ_s^j denotes this operator in (10). This operator appears naturally once a linear hypothesis of Onsager type [43,44] is made on the kinetics of the irreversible mechanisms. It takes the form

$$\dot{\mathbf{z}} = \mathbf{L} \mathbf{A} \quad (11)$$

to link linearly the fluxes and forces of internal processes. Besides and according to (8), the relaxed state condition leads to

$$-\mathbf{g}(\boldsymbol{\gamma}, \mathbf{z}^r) \dot{\mathbf{z}}^r = {}^t \mathbf{b}(\boldsymbol{\gamma}, \mathbf{z}^r) \dot{\boldsymbol{\gamma}} \quad (12)$$

The combination of the two preceding equation along with (8b) allows to write

$$\dot{\mathbf{A}} = -\mathbf{g}(\dot{\mathbf{z}} - \dot{\mathbf{z}}^r) \quad (13)$$

which, with proper integration in time with reference to the equilibrium state (and classical assumptions regarding the dependence of matrix \mathbf{g} with respect to \mathbf{z} variables) leads to $\mathbf{A} = -\mathbf{g}(\mathbf{z} - \mathbf{z}^r)$ and hence, using relation (11) to

$$\dot{\mathbf{z}} = -\mathbf{L} \mathbf{g}(\mathbf{z} - \mathbf{z}^r) = -\boldsymbol{\tau}_z^{-1}(\mathbf{z} - \mathbf{z}^r) \quad (14)$$

Using the same notations for matrix \mathbf{L} and \mathbf{g} , properties of this operator of relaxation times are discussed especially in [16,18,40]. It has been shown by Meixner [39] that this matrix can be diagonalized in an appropriate space (the space of dissipations or the 'Onsager' space in [32]), introducing a modal analysis of relaxation through an appropriate relaxation times spectrum. Once again, such analysis has been made in the past by thermodynamicists but was also historically due to chemists (Jouguet's theorem relative to the dynamics of chemical reactions and the diagonalization of the matrix representing the stoichiometric coefficients of independent reactions). Without going into deep details here (refer to e.g., [3,14,15]), the space of dissipations is appropriate to model the regression of fluctuations near equilibrium. The fluctuation-dissipation theorem [18,45] relies on the principle of equipartition of the created entropy according which, each dissipative mode associated with the process of creation of the fluctuation produces on average the same dissipation. This lead Cunat [14] to propose a distribution law for the relaxation times of the modal spectrum. The weights p^j are introduced to describe the influence of each mode of relaxation j on the global behavior (Letter j refers not anymore to various unknowns or badly defined chemical reactions but to different modes of relaxation). The application of the fluctuation-dissipation theorem produces a relationship between the weights p^j and corresponding relaxation times τ^j that is given by $p^j = B \sqrt{\tau^j}$ where B is obtained thanks to the normalization condition $\sum_j p^j = 1$. Going back to (10) for example, the dissipative component of the state equations introduces variables $\beta^j = p^j \boldsymbol{\beta}$ and $\beta^{j,r} = p^j \boldsymbol{\beta}^r$. For calculations in practical applications, a relaxation times spectrum is defined by its maximum relaxation time τ_{max} and its width (number of decades in a logarithmic approach) to get directly the weight p^j associated to each mode.

From the thermodynamics of constitutive laws

The final step leads us to the heat transfer equation governing a REV behavior, with a full description of the various contributions introduced by the thermodynamical formalism described above. The state equation (9) for the entropy rate evolution is combined with the entropy balance (4) that leads to:

$$\dot{s} = \frac{A \cdot \dot{z}}{T} + \frac{\lambda \Delta T}{T} = \left(\frac{\rho C_u}{T} \dot{T} + \alpha_u E_u \dot{\varepsilon} \right) - \sum_j \frac{(p^j s) - (p^j s^r)}{\tau_s^j} \quad (15)$$

and by rearranging terms makes rise the heat equation

$$C_u \dot{T} = \lambda \Delta T - \alpha_u E_u T \dot{\varepsilon} + \sum_j \left(\frac{s^j - s^{j,r}}{\tau_s^j} \right) T + A \cdot \dot{z} = \lambda \Delta T + \dot{q}(x, y, t) \quad (16)$$

with, in order of appearance, the accumulation term, the Fourier Laplacian, and a heat source term $q(x, y, t)$ which made clear the three contributions q_1, q_2, q_3 originating from the thermomechanical couplings:

- $\dot{q}_1 = -\alpha_u E_u T \dot{\varepsilon}$ for the thermoelastic instantaneous coupling,
- $\dot{q}_2 = \sum_j \left(\frac{s^j - s^{j,r}}{\tau_s^j} \right) T$ for the differed inelastic coupling between entropy and 'internal' dissipative variables,
- $\dot{q}_3 = A \cdot \dot{z} = \mathcal{D}$ for the dissipative component (couplings between 'internal' variables themselves).

3.3 Methods used for solving the IHCP

Equation (16) states the direct model of the problem along with Dirichlet boundary conditions, since the contour temperatures will be known (also noisy) as a result of the measurement. The inverse problem consists in estimating the source term $\dot{q}(x, y, t)$. Two techniques have been developed based on the minimization of the quadratic distance between the measured temperature field and its modeled counterpart. Due to the ill-posed nature of such a problem, some regularization process has been introduced that yields an approximate but more stable solution. Both methods are fully described in [48,49] and therefore; only few information is given here.

- Method 1 (Algorithm A1) is based on a constrained optimization. The direct model appears as an applied constraint like in [47,59] and a Tikhonov-type regularization [57] has been adopted (regularization by penalization).
- Method 2 (Algorithm A2) is based on an analytical solution of the direct problem obtained by transforming (16) in the Laplace-Fourier transformed domain (spectral approach). Like for classical heat transfer problems where Laplace-Fourier integral transforms are applied [36], a linear relationship is obtained between the transformed temperature and the transformed internal heat source function. Regularization is achieved by combining two tools: A "Future times step" regularization procedure [6] is used for temporal smoothing of the solution. Another regularization is achieved by appropriate truncation on the spatial modes (diminishing the number of modes reduce the number of degrees of freedom on the approximated function). No additional constraint under the form of a penalty term is added to the objective function.

These two methods are based on really distinct approaches for solving the IHCP and have been proved to give identical results in inversion tests based on theoretical simulations [49]. In the present paper, application is made on real thermomechanical data.

4 Inversion of real data in uniaxial tension

These algorithms will now be applied to real experimental data. A specimen of HDPE is subjected to a tensile test in the metrological platform exposed in Sect. 2. Every experimentalist knows that working on experimental data brings additional turpitudes compared to inversion on simulated data. Therefore, a specific procedure is generally necessary to get round the problems of 'real life'.

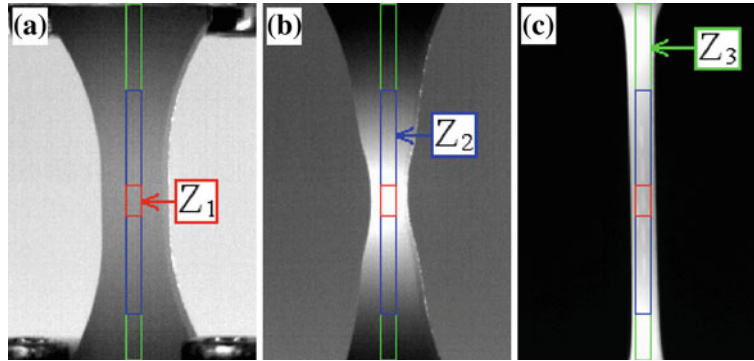


Fig. 4 Details of zones Z_1 , Z_2 , and Z_3 for THS reconstructions

4.1 Adopted procedure

On the Fig. 4 below, we have reproduced the thermal images given by the IR camera at three different times: instant $t = 0$ —non-deformed specimen ($\epsilon_y = 0$), instant $t = 240$ s ($\epsilon_y = 1.21$), instant $t = 385$ s ($\epsilon_y = 1.93$). They illustrate the geometrical problem that makes the inversion difficult. Because of the slender shape of specimens in such tests, a monitoring of the temperature field all over the deformed reference length leads to an observation frame that is very large when compared to the thermal scene under interest. Moreover, the observation zone noted Z_i (domain considered for the source reconstruction) must be based on a material area that has to be defined from the last recorded image. In case not, pixels would be taken into account that would belong initially to the specimen surface but not later because of the necking phenomenon. The frames Z_i drawn on the thermal images meet this requirement. Of course, the consequence of that is the reduced number of pixels really useful for inversion, although the detector array is 320×240 px in size. This matter was accounted for already in the simulation of inversions to assess the performances of the algorithms. Zone Z_1 roughly corresponds to a size of 21×10 px for all experiments. This zone corresponds to the REV on which the stress/strain measurements are obtained. We also have defined zones Z_2 and Z_3 with very slender shapes but larger sizes that will allow us to perform the reconstruction at the scale of the ‘specimen’ structure but also to check the algorithms in a contradictory way. For zone Z_1 of limited extension, both algorithms will be used but only the time-dependent spatially averaged source $\langle \dot{q} \rangle_{Z_1}(t)$ will be identified. A spatially averaged source over a surface of pixels Z is denoted by $\langle \dot{q} \rangle_Z$ and corresponds to $\frac{1}{S_Z} \int_Z \dot{q}(x, y, t) dS$. No regularization is necessary in this case (see [48]). Zones Z_2 and Z_3 are much larger, corresponding, respectively, to 151×11 px and 237×11 px. They will be submitted to a reconstruction process accounting for strong temperature gradients and localization effects of the sources, which follow the necking lips displacement during the extension. The spatial reconstruction imposes here a regularization, and we will be able to verify whether, for example in the case of Z_2 , $\langle \dot{q}_{Z_2}(x, y) \rangle_{Z_1} = \langle \dot{q} \rangle_{Z_1}$. The choice of zone Z_3 is interesting to check the localization ability of the algorithms.

The results that will be presented below satisfy the conditions of optimal identification as defined in the previous theoretical works [48,49] especially with respect to the regularization. Algorithms A1 and A2 are used in a 1-D version according to the slender shape of the specimen—especially in deformed state (Fig. 4)—and the very oriented 2D temperature fields observed experimentally in the tensile direction (longitudinal and transversal profiles shown on Fig. 5). Applying 2D algorithms would yield inconsistent results as will be seen later. The experiment corresponds to a strain rate $\dot{\epsilon}_y = 0.005$ s $^{-1}$. Two longitudinal profiles are given for $\epsilon_y = 1.2$ at time $t = 240$ s and $\epsilon_y = 1.6$, $t = 320$ s (cf. Fig. 5a). For a deformation of $\epsilon_y = 1.6$, nine transverse profiles have been plotted. One of them corresponds to the central area of interest and the remaining ones correspond to the 2×4 profiles taken symmetrically with respect to this center (vertical lines plotted on the longitudinal profiles). One can note significant temperature differences (of the order of 3C) on the longitudinal profiles where at the same time, transverse profiles show a flat uniform behavior (within the measurement noise, Fig. 5b). Considering longitudinal profiles of Fig. 5a, the signal to noise ratio is most favorable to the use of 1D algorithms. Moreover, it can be substantially enhanced thanks to a legitimate averaging of the temperature profiles along the transverse direction.

Finally, according to the expected Biot numbers of the order of 0.1 or less, direct simulations have shown that the sensitivity to the heat exchanges with the surroundings in the fin approximation is very small. Identifications have been carried on without considering such parameter (set to a zero value).

From the thermodynamics of constitutive laws

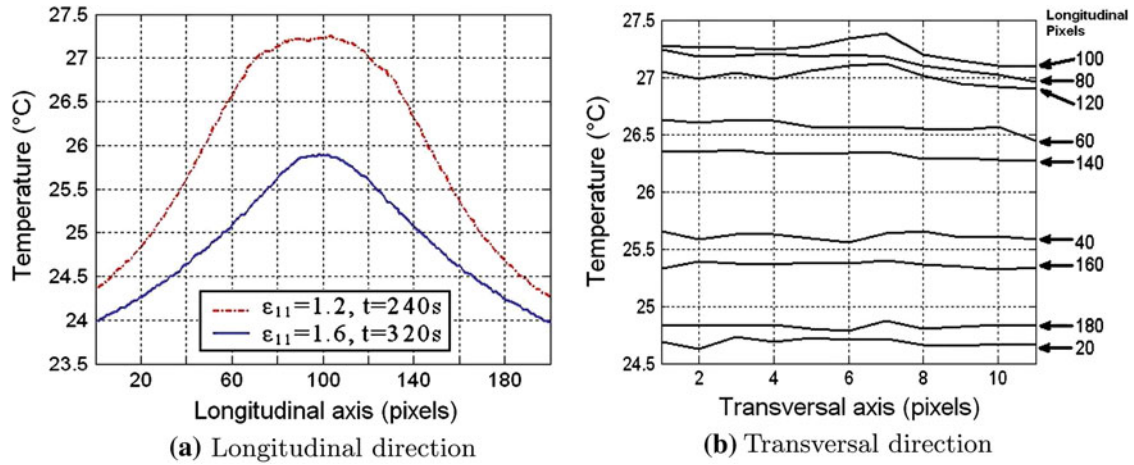


Fig. 5 Temperature profiles (test at $\dot{\epsilon}_y = 0.005 \text{ s}^{-1}$). **a** Longitudinal direction. **b** Transversal direction

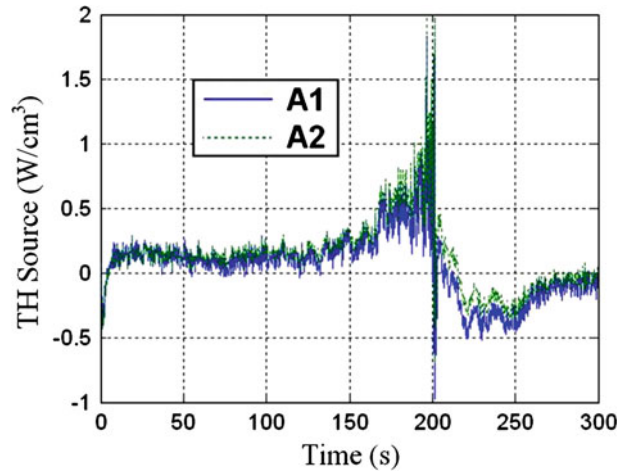


Fig. 6 Identification of 1D THS using algorithms A1 and A2 on Z_1 ($\dot{\epsilon}_y = 0.01 \text{ s}^{-1}$)

4.2 Identification of experimental THS

Figure 6 shows the temporal evolution of the THS $\langle \dot{q} \rangle_{Z_1}(t)$ identified from algorithms A1 and A2 on zone Z_1 (without regularization). We can first notice that both algorithms give the same result. Figure 6 corresponds to an experiment performed at a strain rate ($\dot{\epsilon}_y = 0.01 \text{ s}^{-1}$), but all the identifications obtained at different strain rates confirm the independence of the results with respect to the algorithms used. Looking at the physical content of the result leads to the conclusion that the estimated THS presents a consistent behavior with respect to what is more or less expected. The negative source in the initial times corresponds to the instantaneous thermoelastic coupling (proportional to the strain rate). A strong elevation of the thermal power follows that makes it positive and relatively constant in the plastic regime, after a slight overshoot around the yield stress. At high deformations, in the hardening phase that corresponds to fibrillation of the polymer [9], the THS source increases. In the relaxation phase (when tension is stopped while the strain is maintained constant), the result is at first sight surprising: the THS becomes rapidly negative, passes through an extremum, and then goes back to zero, as expected from the thermodynamics of equilibrium of two systems (specimen and surrounding air) in contact. The apparent endothermic behavior of the THS will be explained later thanks to the thermodynamical model described in Sect. 3.2.

Now, we consider the identification of the THS on zone Z_3 . Over this area, a regularizing procedure is used in order to rebuild the THS field. The parameters of the regularization for algorithm A2 are the number of spatial modes n_i and of future times step n_{tf} . They are optimized at values, respectively, equal to $n_i^y = 120$ in the y -spatial direction, $n_i^x = 6$ in the x -spatial direction (only for 2D reconstruction) and $n_{tf} = 15$.

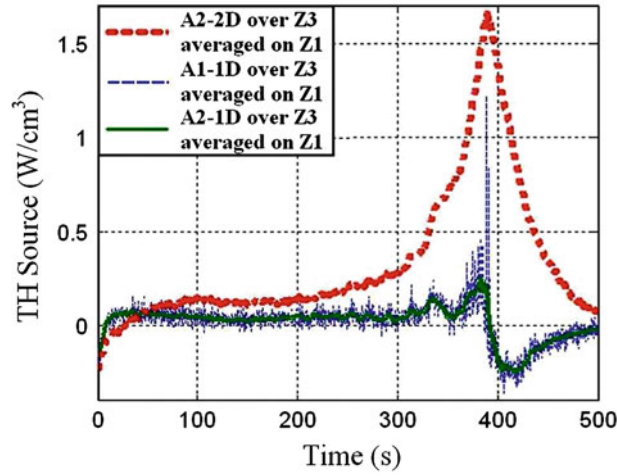


Fig. 7 Identification of 1D and 2D THS on zones Z_1 and Z_3 ($\dot{\epsilon}_y = 0.005 \text{ s}^{-1}$)

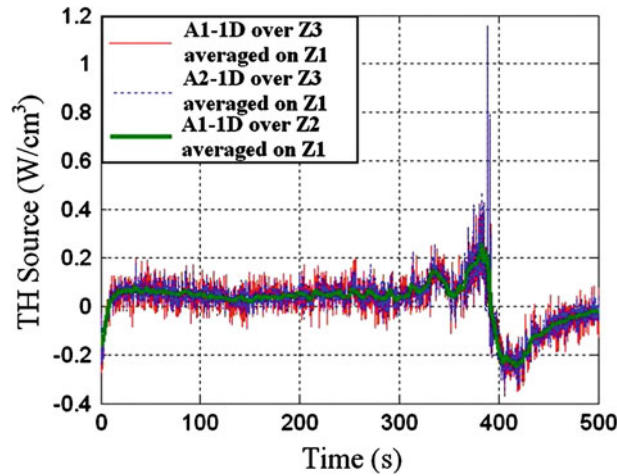


Fig. 8 Comparison between THS identified on Z_1 with the 1-D algorithms applied on zones Z_2 and Z_3 ($\dot{\epsilon}_y = 0.005 \text{ s}^{-1}$)

Next, the identified source field for each point (pixel) of ‘window’ Z_1 (central part of the specimen) is averaged in order to get $\langle \dot{q}_{Z_3}^{2D}(x, y) \rangle_{Z_1}$. The same operation is carried on with the 1D algorithms: we identify the estimated source profile $\dot{q}_{Z_3}^{1D}(y)$ over area Z_3 and then, compute the averaged over zone Z_1 $\langle \dot{q}_{Z_3}^{1D}(y) \rangle_{Z_1}$. Figure 7 shows that the averaged identified sources on the REV (Z_1) from the 1D algorithms applied on zone Z_3 produce the exact same results. The smoothing effect of the future times procedure in A2 can be clearly seen on this figure when one compares the source signals produced by A1 and A2. It can be also remarked from the figure that, as previously discussed, the 2D identification fails and does not give the same behavior as obtained with the 1D algorithms. The very strong 1D character of the temperature field (and of the transfer itself) is of course responsible for this lack of efficiency of 2D algorithms. The use of zone Z_2 allows to assess the consistency of the reconstruction procedure whatever the considered observation zone and the algorithm used. On Fig. 8, one can verify that we have

$$\langle \dot{q}_{Z_3}^{1D}(y) \rangle_{Z_1} = \langle \dot{q}_{Z_2}^{1D}(y) \rangle_{Z_1} = \langle \dot{q} \rangle_{Z_1} \quad (17)$$

The local sources identified on Z_2 and Z_3 and then averaged on Z_1 give back the averaged source directly estimated on Z_1 .

Finally, a representation of the 1D THS profiles all along the experiment can be obtained Fig. 9b from the temperature maps Fig. 9a recorded during the test ($\dot{\epsilon}_y = 0.01 \text{ s}^{-1}$). Such results are very original when looking at the literature on the subject. They illustrate that the localization effects of the source can be efficiently

From the thermodynamics of constitutive laws

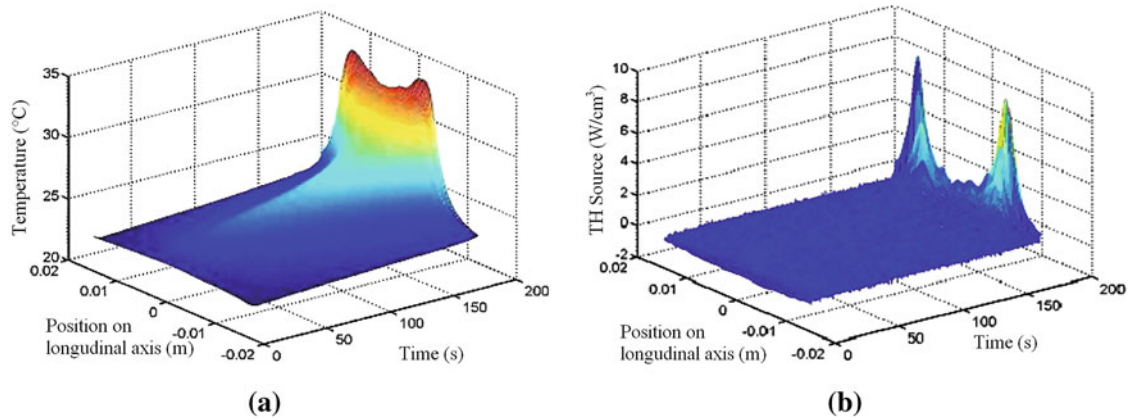


Fig. 9 Temperature and TH Source maps (test at $\dot{\epsilon}_y = 0.01 \text{ s}^{-1}$). **a** Temperature. **b** THS

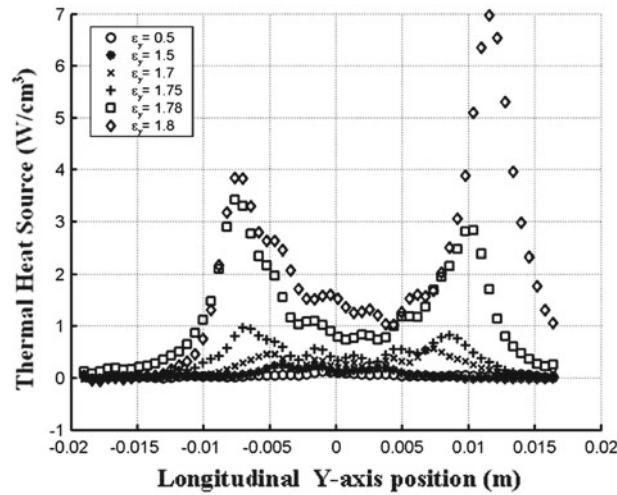


Fig. 10 Reconstructed THS profile at different strains for a tensile test at $\dot{\epsilon}_y = 0.01 \text{ s}^{-1}$

extracted from the smooth temperature profiles. The localization of thermomechanical mechanisms appears clearly in the central part of the specimen when necking initiates but the THS power remains small (around 0.10 W/cm^3). For very high plastic deformation, the manifestation of hardening occurs simultaneously with a splitting of the necking lips in direction of the grips: matter necessary for further plastic flow is produced by a disintegration of the microstructure in the lips. Figure 10 provides profile plots of the reconstructed THS along the tensile direction at different strains. It makes more clear the development of strong heat effects in the necking lips at high deformations, which suggests that the mechanisms initiated during the necking in the central part of the specimen are likely different than those when the necking propagates.

5 Physical interpretation

A critical analysis of the results given by the reconstruction algorithms and the experimental data can be made in two ways. The first one consists in verifying whether the thermal information is really pertinent as a manifestation of deformation micromechanisms at stake in the material. This has been made in [5]. The second one aims at applying the thermodynamical model developed earlier in order to check its ability to reproduce the thermomechanical observables. This can be done directly by using a new inverse procedure (Levenberg-Marquardt algorithm) in order to estimate the parameters of the model. Only one typical result will be given as the aim of this section is firstly to show that the mathematical structure of the behavioral model we used (in its most reduced form, i.e., with the minimum number of parameters) is able to capture the observations, and secondly, to show how the model can now be used to investigate the different thermomechanical couplings.

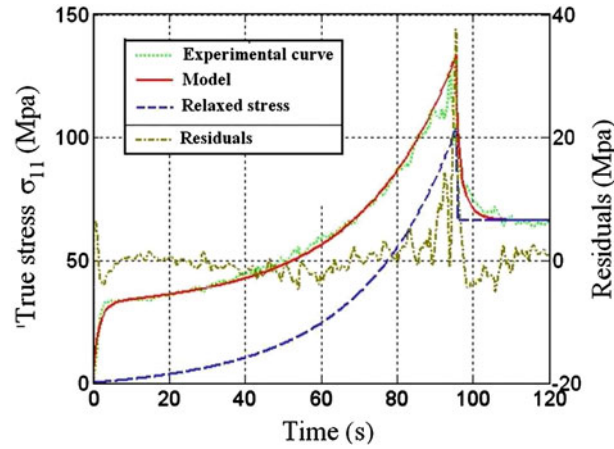


Fig. 11 Experimental and theoretical fitted curves $\sigma = f(t)$ for the tensile-relaxation test at $\dot{\epsilon}_1$

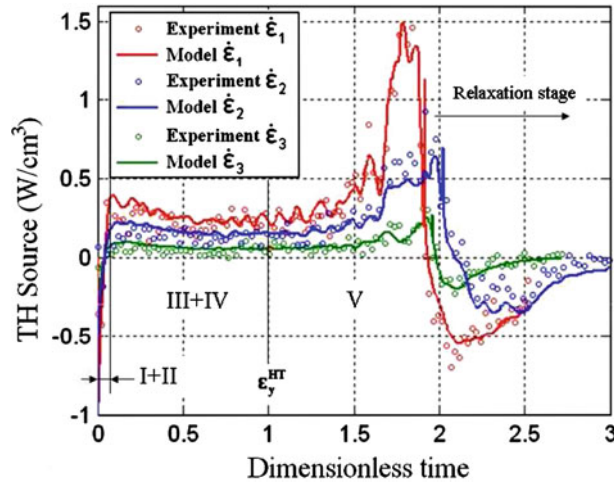


Fig. 12 Experimental and theoretical fitted curves $q = f(t)$ for the tensile-relaxation test at three different strain rates

5.1 Physical analysis of the results

Figures 11 and 12 show the results obtained for different tensile experiments. Figure 11 plots the mechanical observable, the true stress obtained for a true longitudinal strain rate of $\dot{\epsilon}_y = 0.02 \text{ s}^{-1}$ as a function of time t . At a deformation of 1.87, a relaxation is imposed to the specimen. One recognizes the typical behavior of HDPE that can be divided into three phases: at low strains, a strong quasi-elastic increase of the stress (Phase I and II) is observed. At the yield stress (of the order of 50 MPa), the stress–time curve stabilizes, which corresponds to the plastic regime of deformation (phase III and IV). Finally, a hardening phase occurs (phase V). Once a strain of 1.87 is reached, it is maintained constant. During this relaxation phase, the stress decreases from 120 to 60 MPa. Figure 12 plots the thermomechanical observable, the THS obtained for the following three tensile strain rates $\dot{\epsilon}_y$:

$$\dot{\epsilon}_1 = 2 \cdot 10^{-2} \text{ s}^{-1}, \dot{\epsilon}_2 = 10^{-2} \text{ s}^{-1}, \dot{\epsilon}_3 = 5 \cdot 10^{-3} \text{ s}^{-1}$$

One can first notice the difference that exists between the two signals in terms of noise. This illustrates the difficulty of the metrological task. Having the same measurement quality (resolution and numerical levels of both video and IR cameras), the mechanical signal results from a direct physical measurement while the thermomechanical signal is the double result of a measurement and of a difficult inversion process that generally increases the level of noise. Nevertheless, a good reproducibility of the data has been observed [5]. The thermal processes accompanying the deformation can be analyzed, and four distinct phases can be distinguished.

At short times (instantaneously), the THS is negative. This endothermic effect is the manifestation of the reversible phenomena associated to thermoelasticity and well known since the early studies on the ideal gas (phase I). The intensity of the source is theoretically equals to $\alpha_u E_u T_0 \dot{\varepsilon}$. This has been confirmed, the identified THS being always perfectly proportional to the strain rate.

In a second stage, mechanical processes at stake suddenly become strongly exothermic. The THS becomes positive in a very few seconds (Phase II) and reaches its maximum when necking sets in. The microstructural mechanisms induced strong thermal effects in this phase and may correspond to transformations of the crystalline phase as observed by manu authors through X-Ray diffraction.

The THS remains quasi constant during stages III and IV corresponding to the plastic flow regime. The value is stabilized around a power of 0.18 W/cm^3 for strain rates of 0.005 and 0.01 s^{-1} .

The initiation of the hardening stage (Phase V) can be clearly seen on the THS signal as it corresponds to a new increase in intensity. It is obtained for a strain of $\varepsilon_y^H \approx 1$. Note that this strong increase in power is observed in the central region of the specimen (the REV). It does not correspond to the much higher THS recorded on the profile (see Fig. 10), which occurs in the necking regions (that have moved symmetrically from the central zone for such large strains). In the hardening phase, additional mechanisms take place in the matter at microstructural level like the elongation of the fibrils formed during stages III and IV [27].

During the relaxation, an interesting phenomenon is observed. Once relaxation is initiated, the THS decreases very rapidly and becomes negative. A minimum is reached and then the THS returns to 0 as expected for long times. This strong cooling of the specimen corresponds to a strong extra energy removing (much greater than the simple cooling due to heat exchanges). The thermodynamical model allows to identify this energy to a variation of entropy as a function of time (next section). Just like for the stress, the entropy of the system placed in non-equilibrium conditions evolved toward a relaxed state (or entropy s^r) according to the kinetic described with the relaxation spectrum τ_s^j .

5.2 Constitutive equations for parameter identification

According to the mathematical structure of the modeling (8), the following equations are obtained from the thermodynamical model with $\dot{\beta} = [\dot{s}, \dot{\sigma}]$:

$$\dot{s}^j = p^j \left(\frac{\rho C_u}{T} \dot{T} + \alpha_u E_u \dot{\varepsilon} \right) - \frac{(s^j) - (s^{j,r})}{\tau_s^j} \quad (18a)$$

$$\dot{\sigma}^j = -p^j \alpha_u E_u \dot{T} + p^j E_u \dot{\varepsilon} - \frac{\sigma^j - \sigma^{j,r}}{\tau_\sigma^j} \quad (18b)$$

$$\frac{1}{2} \ddot{q}_3^j = -\dot{T} \frac{s^j - s^{j,r}}{\tau_s^j} + \dot{\varepsilon} \frac{\sigma^j - \sigma^{j,r}}{\tau_\sigma^j} - \frac{\dot{q}_3^j}{\tau_{q_3}^j} \quad (18c)$$

All these equations are written for one given mode j , and the global response can be calculated by summation.

The first equation corresponds to the state equation of the entropy already shown in (9). The relaxed state for the entropy is described by a constant apparent relaxed heat capacity (most simple approach minimizing the total number of parameters of the model). Thus, $s^r = \rho C_r \log(T/T_0)$ where T_0 is the initial temperature. The relaxation times spectrum τ_s^j is characterized by only one parameter: the maximum relaxation time τ_{max}^s (the number of decades is fixed at a constant value, see explanation below).

The second equation corresponds to the state equation of the stress. A different linear spectrum is used for the relaxation times of the mechanical component (τ_σ^j) as the microscopic processes may be different than those of the thermal component. The relaxed state for the stress during drawing is described using the Haward-Thackray model: $\sigma^r = E_h \varepsilon_{HT}$ where E_h designates an hyperelastic modulus and ε_{HT} is a deformation variable defined in [26] as $\varepsilon_{HT} = \exp(2\varepsilon) - \exp(-\varepsilon)$. The identification will be performed in the case of a tensile-relaxation test. The tensile test at constant strain rate $\dot{\varepsilon}$ is imposed to the HDPE specimen until a strain of $\varepsilon_r \simeq 1.9$ is reached. Then, the strain is maintained constant allowing for the relaxation of the stress. In this relaxation phase, the relaxed state for the stress will be described by a constant value $\sigma^{j,r} = p^j \sigma^{eq}$.

The remaining last (18c) describes the evolution of the dissipation function $q_3 = A\dot{z}$. It can be deduced from the thermomechanical model in a very straightforward manner (demonstration not given here) starting from the evolution law of the Affinity (8) and using Onsager's law (11). The independence of the Onsager

Table 1 Thermomechanical parameters identified on tensile-relaxation tests

	$\dot{\epsilon}_1$	$\dot{\epsilon}_2$	$\dot{\epsilon}_3$
Eu (MPa)	2,276		
E_h (MPa)	2.28		
$\tau_{\max,T}$ (s)	1.953	3.93	7.25
$\tau_{\max,R}$ (s)	2.92	4.96	16.88
σ^{eq} (MPa) (s)	66.0	75.2	68.7
ρC_u (J/m ³ /K)	1.724×10^6 known		
α_u (K ⁻¹)	16×10^{-5} known		
ρC_r (J/m ³ /K)	0.33×10^6		
$\tau_{\max,T}^s$ (s)	0.48	1.48	2.43
$\tau_{\max,R}^s$ (s)	1.03	6.98	10.97

kinetic coefficients L^j with respect to time is the only assumption to make. Note that a characteristic time τ_{q_3} for the dissipation naturally appears. In the estimation procedure, we will consider as a first step that both relaxation spectrum τ_s and τ_{q_3} will be identical (same number of decades and same maximum time τ_{\max}). Thanks to the entropy balance made previously (16), this set of three state equations is completed by the THS (19) below.

$$\dot{q}(t) = \dot{q}_1(t) + \dot{q}_2(t) + \dot{q}_3(t) = -\alpha_u E_u T \dot{\epsilon} + \sum_j \left(\frac{s^j - s^{j,r}}{\tau_s^j} \right) T + A \cdot \dot{z} \quad (19)$$

These four equations allow us to calculate:

- the observable $\dot{\sigma}(\dot{\epsilon}, \dot{T})$ through direct calculations from (18b)
- the THS observable reconstructed from the thermal images $\dot{q}(\dot{\epsilon}, \dot{T})$ through the calculation of (19) from the solutions of (18).

The input vector $(\dot{\epsilon}, \dot{T})$ is known, as $\dot{\epsilon}$ is the command of the tensile machine and \dot{T} is measured using the local averaging of the temperature map on the REV. The choices or assumptions made to describe the relaxation spectrum or the relaxed state have led to a reduced model, i.e., a model using a minimum number of sensitive parameters (parsimony principle). The aim of parameter estimation is to obtain precise and uncorrelated values of the parameters from an adjustment between experimental and modeled data. This is always possible when an optimum compromise is reached between a reduced model—capturing the basic physical features of the phenomenon to describe—and the number of parameters to estimate. Respecting this methodology, one may judge the hypothesis made to establish the model (in our case the relaxed state and relaxation times spectrum)

5.3 Identified parameters of the model

In a first step, only the mechanical observable (stress–strain curve) is considered. The parameter vector is $\{Eu, E_h, \tau_{\max,T}, \tau_{\max,R}, \sigma^{\text{eq}}\}$ where subscripts T, R for the relaxation times denote the tensile or relaxation phases of the test. A sensitivity analysis has shown that these parameters are all uncorrelated and have comparable sensitivities [8]. The estimated variance on all parameters is smaller than 3%. It has also led to consider a spectrum of $N = 7$ decades (for both tensile and relaxation stages). Indeed, this parameter has been removed as it appears correlated with the maximum time of the spectrum and with the Young modulus when it is too low. When it is set to a sufficiently high value, on the contrary, its sensitivity becomes null, and the remaining parameters are well estimated. The estimation is performed using Levenberg-Marquardt algorithm. Table 1 reports the identified values for the three strain rates $\dot{\epsilon}_1, \dot{\epsilon}_2, \dot{\epsilon}_3$. For the Young modulus value Eu , a very different value is found compared to the one given by the manufacturer (Röchling HDPE: $Eu = 1,200$ MPa !). Of course, it was probably obtained using the standards ISO 527-1 or ASTM D638, which give a protocol for determining elastic modulus on polymers with a linear assumption although the behavior is viscoelastic since the earliest times. The value we obtained by a real estimation procedure based on a data-fitting procedure applied to the stress-strain curve is then twice the value of the manufacturer. It is independent of the strain rate of the test. This value has been confirmed by measurements made independently (other labs) using two different techniques. A value of $Eu = 2.32^{\pm 0.15}$ GPa has been obtained using an ultrasound technique (pulse-echo technique at $f = 5$ MHz, see e.g., [35]), which is possible on semicrystalline materials. A value of $Eu = 2.52^{\pm 0.07}$ GPa

has been obtained by the continuous stiffness method [34] applied with a nanoindenter IIS (average of 15 measurements taken at 20 μm of distance and indents of depth varying from 0.5 to 4 μm). Concerning the hyperelastic modulus, its estimated value was $E_h = 2.28 \text{ MPa}$, which is three orders of magnitude smaller than the elastic modulus. It corresponds to the range of data available in the literature for HDPE [25]. Concerning the maximum relaxation times $\tau_{\max, T}$ obtained during traction, it is interesting to observe that they are all the more smaller as the strain rate grows, as physically expected. It is also noticeable that, corrected from the strain rate, these times lead to a unique constant Deborah number: $De^1 = 0.0391$, $De^2 = 0.0393$, $De^3 = 0.0363$ within a 8% of scatter. This means that a simple linear distribution of relaxation times is sufficient to describe the behavior of the polymer from the elastic to hyperelastic behavior. The data-fitting procedure is of good quality as can be seen in Fig. 11. The experimental curve (dots) is plotted along with the modeled one at convergence of the estimation. The curve corresponding to the right-hand side label, centered on a zero value, corresponds to the identification residuals (discrepancy between experimental and modeled data). This curve shows how well the model fits the data. It is not biased (centered residuals) and describes both the tensile and relaxation stages.

In a second step, the THS is used to complete the identification of the parameters of the thermomechanical law. The mechanical parameters are assumed known. The thermomechanical coupling imposes additional parameters. Among them, parameters ρC_u and α_u will be assumed known. A value of $\rho C_u = 1,724,000 \text{ J/m}^3/\text{K}$ was precisely determined by calorimetry using a home-made apparatus developed in the thermal sciences research team at LEMTA laboratory. The thermoelastic coefficient $\alpha_u = 16 \times 10^{-5} \text{ K}^{-1}$ was estimated directly on the THS reconstructed signal from the magnitude of the negative heat source peak observed instantaneously and given by $\dot{q}_1 = \alpha_u E_u T_0 \dot{\epsilon}$. This value is close to that of the manufacturer ($20 \times 10^{-5} \text{ K}^{-1}$). It remains three thermomechanical parameters to identify: $\{\rho C_r, \tau_{\max, T}^s, \tau_{\max, R}^s\}$. The same number of decades as for the mechanical signal was considered for the thermomechanical equations (18(a), 18(c)).

The sensitivity analysis shows that these three coefficients are always perfectly identifiable. The variance-covariance matrix is excellent with estimated variances on the parameters smaller than 1% and correlation coefficients very small compared to 1. Figure 11 shows the fitted curves obtained for the three different strain rates. Table 1 gives the identified values. It is worthwhile to mention that the relaxed state for entropy s^r is normally described through the knowledge of both a relaxed coefficient for the heat capacity ρC_r and for the dilatometric coefficient α_r . In the absence of any valuable information on these two coefficients, the entropy in the relaxed state was considered as constant, independent of the strain rate and governed only by the heat capacity in relaxed state. In other words, a value of $\alpha_r = 0$ has been considered to perform the identification and the heat capacity in relaxed state plays the role of an apparent quantity. As a consequence, no physical meaning must be sought of the value found for ρC_r at the moment. One can also quote that the order of magnitude of the identified relaxation times is respected: smaller times with increasing rates, smaller times in tension than in relaxation.

Finally, one can focus on the interesting question of the relative magnitude of the three thermomechanical couplings that contribute to the THS. Thanks to the model and the identification process, it is now possible to calculate the evolution of \dot{q}_1 , \dot{q}_2 , and \dot{q}_3 versus time during the all test. These are plotted on Fig. 13 for the strain rate $\dot{\epsilon}_1$ and along with the experimentally determined overall THS. The three following comments can be made:

- Dissipation \mathcal{D} or \dot{q}_3 is always identified as strictly positive. It cancels as soon as the mechanical excitation is stopped but has required some time to be established. It reaches a maximum value at the yield point. It is also important to note that it stabilizes in the plastic regime to a constant value that corresponds exactly to the global THS. This means that in this regime, it weighs in strongly on the overall THS (quasi 100%). According to the model, the thermoelastic and entropic couplings compensate themselves in the plastic flow regime. Apart from these first qualitative features, identifying the THS in this regime to a pure intrinsic dissipation of Rayleigh type calculated by the means of an apparent viscosity according to $\dot{q}_3 \approx \eta \dot{\epsilon}^2$ leads to a value of $20 \cdot 10^8 \text{ Pa.s}$. This corresponds for example to the viscosity of a sodo-silicate glass at the vitreous transition temperature around 600°C . According to the identified values of the Young modulus, this leads to an average characteristic time of the order of $\frac{\eta}{E_u} = \frac{20 \cdot 10^8}{2.27 \cdot 10^9} \approx 1 \text{ second}$, which is nearly the average barycenter of the spectral distribution times identified with the model and which maximum identified time was $\tau_{\max} = 2s$ (Table 1).
- The magnitude of the entropic coupling \dot{q}_2 is set by the identified value of the relaxed heat capacity C_r . As said before, it can be observed that this term compensates the thermoelastic coupling but also includes additional contributions due to thermomechanical relaxations. It is this term that explains the slight overshoot of the THS in the vicinity of the yield point and the strong increase of heat produced in the hardening phase

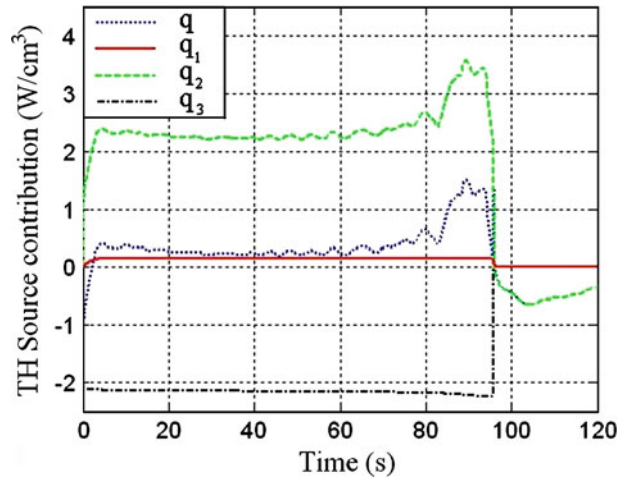


Fig. 13 Theoretical curve $\dot{q} = f(t)$ for the tensile-relaxation test at $\dot{\epsilon}_1$ and behavior of the thermomechanical components \dot{q}_1 , \dot{q}_2 and \dot{q}_3

that has been shown to be linked to a strong deformation of the fibrils. Finally, it is this term that explains the endothermic effect observed as soon as the mechanical excitation is stopped (relaxation phase).

- The thermoelastic effect \dot{q}_1 is very strong. It is of course constant during the tensile phase and stops as soon as the relaxation phase is launched.

For the present time and according to the assumptions of the modeling, these results can be only considered as qualitatively satisfying and consistent with each other. Additional experiments on various materials, a deep analysis of the profound signification of these results in connection to the assumptions made, must be carried on in the future to check the validity of this approach. Our main purpose was to show that the model structure is able to reproduce the reality with a minimum number of parameters.

6 Concluding remarks and perspectives

Starting from infrared images obtained during a tensile test applied on a polymer specimen, the inverse heat source reconstruction problem has been solved using two methods, very different in their approach and in the way regularization is achieved. The thermal images are treated with both algorithms, and equal reconstructed THS are obtained, which assessed the inverse solution. Among the important facts that can be quoted about this work, one can cite:

- regularization is obviously essential to get local behaviors of the THS.
- 2-D algorithms are not necessary in our case (specimen with highly slender shape). Used inappropriately, they can introduce a strong error in the reconstruction.
- 1-D algorithms allow for a good reconstruction of the THS when local phenomena of concentrated sources exists (hot spots appearing in the necking lips for very high strains).
- 1-D algorithms applied on the full length of the specimen have proved that the THS identified for the central reference REV is strictly equal to the average THS reconstructed on this zone without using any regularization procedure. This confirms once again the good reconstruction obtained in the presence of heat conduction.

Finally, the reconstructed THS are confronted to a thermomechanical modeling of the behavior of such a complex material with semicrystalline microstructure. This constitutes a rare attempt in this field. The proposed behavior's law is able, in reduced form, to describe both mechanical and thermal signals. The parameter of the models is identified by appropriate fitting of the data. This finally allows to calculate the respective contribution of the three different thermomechanical couplings. The benefits that can be taken from this in view of a deeper understanding of the physical processes that operates at a microscale level have been clearly shown.

References

1. Adams, G., Farris, R.: Latent energy of deformation of bisphenol a polycarbonate. *J. Polym. Sci. Part B. Polym. Phys.* **26**, 433–445 (1988)
2. Allen, D.: A prediction of heat generation in a thermoviscoplastic uniaxial bar. *Int. J. Solids Struct.* **21**(4), 325–342 (1986)
3. André, S., Meshaka, Y., Cunat, C.: Rheological constitutive equation of solids: a link between models based on irreversible thermodynamics and on fractional order derivative equations. *Rheol. Acta* **42**, 500–515 (2003)
4. Andre, S., Baravian, C., Renault, N., Cunat, C.: In situ mechanical characterization of polymers with the association of three optical techniques. *Appl. Phys. Lett.* **91**(7), 071919 (2007)
5. Baravian, C., Andre, S., Renault, N., Moumini, N., Cunat, C.: Optical techniques for in situ dynamical investigation of plastic damage. *Rheol. Acta* **47**, 555–564 (2008)
6. Beck, J., Blackwell, B., St. Clair, C.: *Inverse Heat Conduction: Ill-Posed Problems*. Wiley-Interscience, New York (1985)
7. Bever, M., Holt, D., Titchener, A.: The stored energy of cold work. *Prog. Mat. Sci.* **15**, 1–190 (1973)
8. Blaise, A., André, S., Delobelle, P., Meshaka, S., Cunat, C.: Identification of the true elastic modulus of high density polyethylene from tensile tests using an appropriate reduced model of the elasto-visco-plastic behavior. *Eur. J. Mech. A/Solids* (2011). Revised manuscript under review
9. Blaise, A., Baravian, C., Andre, S., Dillet, J., Michot, L.J., Mokso, R.: Investigation of the mesostructure of a mechanically deformed hdpe by synchrotron microtomography. *Macromolecules* **43**(19), 8143–8152 (2010). <http://pubs.acs.org/doi/abs/10.1021/ma101033b>
10. Callen, H.: *Thermodynamics*. Wiley, New Jersey (1966)
11. Chrysochoos, A., Belmahjoub, F.: Thermographic analysis of thermomechanical couplings. *Arch. Mech.* **44.1**, 55–68 (1992)
12. Chrysochoos, A., Louche, H.: An infrared image processing to analyse the calorific effects accompanying strain localisation. *Int. J. Eng. Sci.* **38**(16), 1759–1788 (2000)
13. Coleman, B., Gurtin, M.: Thermomechanics with internal state variables. *J. Chem. Phys.* **47**, 597–613 (1967)
14. Cunat, C.: Thermodynamic treatment of relaxation in frozen-in systems - universality of the fluctuation distribution law for relaxation time. *Z. Phys. Chem. Neue Folge* **157**, 419–423 (1988)
15. Cunat, C.: A thermodynamic theory of relaxation based on a distribution of non-linear processes. *J. Non Cryst. Solids* **131–133**(1), 196–199 (1991)
16. Cunat, C.: The dnlr approach and relaxation phenomena. part i - historical account and dnlr formalism. *Mech. Time Depend. Mater.* **5**, 39–65 (2001)
17. De Donder, T.: *Leçon De Thermodynamique et de Chimie Physique*. Gauthier-Villars, Paris (1920)
18. De Groot, S.R., Mazur, P.: *Non-Equilibrium Thermodynamics*. North-Holland Publishing Co, Amsterdam (1963)
19. Doudard, C., Calloch, S., Hild, F., Roux, S.: Identification of heat source from infrared thermography: Determination of 'self-heating' in a dual-phase steel by using a dog bone sample. *Mech. Mater.* **42**, 55–62 (2010)
20. Farren, W., Taylor, G.: The heat developed during plastic extension of metals. *Proc. Roy. Soc. London* **A107**, 422–451 (1925)
21. G'sell, C., Hiver, J.M., Dahoun, A., Souahi, A.: Video-controlled tensile testing of polymers and metals beyond the necking point. *J. Mater. Sci.* **27**, 5031–5039 (1992)
22. Guo, J., Le Masson, P., Artioukhine, E., Loulou, T., Rogeon, P., Carin, M., Dumons, M., Costa, J.: Estimation of a source term in a two-dimensional heat transfer problem: application to an electron beam welding. *Inverse Probl. Sci. Eng.* **14**(1), 21–38 (2006)
23. Gurtin, M.: *Configurational Forces as Basic Concepts of Continuum Physics*. Springer, New York (2000)
24. Gutman, E.: *Mechanochemistry of Materials*. Cambridge International Science Publishing, Cambridge (1998)
25. Haward, R.: Strain hardening of high density polyethylene. *J. Polym. Sci. Part B Polym. Phys.* **45**, 1090–1099 (2007)
26. Haward, R., Thackray, G.: The use of a mathematical model to describe isothermal stress-strain curves in glassy thermoplastics. *Proc. R. Soc.* **1302**, 453–472 (1968)
27. Hiss, R., Hobeika, S., Lynn, C.S.G.: Network stretching, slip processes, and fragmentation of crystallites during uniaxial drawing of related copolymers. a comparative study. *Macromolecules* **32**, 4390–4403 (1999)
28. Hodowany, J., Ravichandran, G., Rosakis, A., Rosakis, P.: Partition of plastic work into heat and stored energy in metals. *Exp. Mech.* **40**(2), 113–123 (2000)
29. Krapez, J.C., Pacou, D., Gardette, G.: Lock-in thermography and fatigue limit of metals. *Quant. Infrared Thermogr.* **5**, 277–282 (2000)
30. Kratochvil, J., Dillon, O.: Thermodynamics of elastic-plastic materials as a theory with internal state variables. *J. Appl. Phys.* **40**, 3207–3218 (1969)
31. Kröner, E.: *Kontinuums Theorie Der Versetzungen und Eigenspannungen*. Springer, New York (1958)
32. Kuiken, D.: *Thermodynamics of Irreversible Processes, Applications to Diffusion and Rheology*. Wiley, Chichester (1994)
33. Le Niliot, C., Gallet, P.: Infrared thermography applied to the resolution of inverse heat conduction problems: recovery of heat line sources and boundary conditions. *Revue Générale de Thermique* **37**(8), 629–643 (2001)
34. Le Rouzic, J., Delobelle, P., Vairac, P., Cretin, B.: Comparaison of three different scales techniques for the dynamic mechanical characterization of two polymers (pdms and su8). *Eur. Phys. J. Appl. Phys.* **48**, 11201 (2009)
35. Legros, N., Jen, C.K., Ihara, I.: Ultrasonic evaluation and application of oriented polymer rods. *Ultrasonics* **37**, 291–297 (1999)
36. Maillat, D., André, S., Degiovanni, A., Batsale, J.C., Moynes, C.: *Thermal Quadrupoles: Solving the Heat Equation Through Integral Transforms*. John Wiley Sons, New York (2000)
37. Maugin, G.: *The Thermomechanics of Plasticity and Fracture*. Cambridge University Press, Cambridge (1992)
38. Maugin, G., Muschik, W.: Thermodynamics with internal variables. part i general concepts. *J. Non Equilib. Thermodyn.* **19**, 217–249 (1994)
39. Meixner, J.: Thermodynamik und relaxationserscheinungen. *Zeitschrift Naturfoeschung* **4a**, 594–600 (1949)
40. Münster, A.: *Thermodynamique Des Processus Irréversibles*. Institut National des Sciences et Techniques Nucléaires and Presses Universitaires de France Saclay, France (1966)

41. Muschik, W.: Internal variables in non-equilibrium thermodynamics. *J. Non Equilib. Thermodyn.* **15**, 127–137 (1990)
42. Nowick, A.S., Berry, B.S.: *Anelastic Relaxation in Crystalline Solids*. Academic Press, New York (1972)
43. Onsager, L.: Reciprocal relations in irreversible processes (i). *Phys. Rev.* **37**, 405–426 (1931)
44. Onsager, L.: Reciprocal relations in irreversible processes (ii). *Phys. Rev.* **38**, 2265–2279 (1931)
45. Prigogine, I.: *Introduction à la Thermodynamique Des Processus Irréversibles*. DUNOD, Monographies, Paris (1968)
46. Prigogine, I., Defay, R.: *Thermodynamique chimique conformément aux méthodes de Gibbs et De Donder*, Tomes I-II. Gauthier-Villars (1944–1946)
47. Rajic, N.: Thermographic assessment of the heat dissipation associated with fatigue crack growth in mild steel. Tech. Rep. TR-1190, Defence Science & Technology Organisation (2001)
48. Renault, N., André, S., Maillet, D., Cunat, C.: A two-step regularized inverse solution for 2-d heat source reconstruction. *Int. J. Thermal Sci.* **47**(7), 834–847 (2008)
49. Renault, N., André, S., Maillet, D., Cunat, C.: A spectral method for 2d spatial distribution and time history estimation of a thermomechanical heat source from infrared temperature measurements. *Int. J. Thermal Sci.* **49**(8), 1394–1406 (2010)
50. Salamatina, O., Höhne, G., Rudnev, S., Oleinik, E.: Work, heat and stored energy in compressive plastic deformation of glassy polymers. *Thermochim. Acta* **247**, 1–18 (1994)
51. Schapery, R.: A theory of nonlinear thermoviscoelasticity based on irreversible thermodynamics. In: ASME (ed.) *Proceedings of the Fifth US National Congress of Applied Mechanics*, vol. 511, pp. 30–37 (1966)
52. Silva Neto, A., Özisik, N.: The estimation of space and time dependent strength of a volumetric heat source in a one-dimensional plate. *Int. J. Heat Mass Transfer* **37**(6), 909–915 (1994)
53. Staverman, A., Schwarzl, F.: Thermodynamics of viscoelastic behaviour (model theory). *Proc. Acad. Sci.* **B55**, 486–492 (1952)
54. Tauchert, T.: The temperature generated during torsional oscillations in polyethylene rods. *Int. J. Eng. Sci.* **5**, 353–365 (1967)
55. Tauchert, T., Afzal, S.: Heat generated during torsional oscillations of polymethylmethacrylate tubes. *J. Appl. Phys.* **38**(2), 4568–4572 (1967)
56. Taylor, G., Quinney, H.: The latent heat remaining in a metal after cold drawing. *Proc. R. Soc. Lond.* **A163**, 157–181 (1937)
57. Tikhonov, A.: Solution of incorrectly formulated problems and the regularization method. *Soviet Math. Doklady* **4**, 1035–1038 (1963)
58. Tisza, L.: *Generalized Thermodynamics*. M.I.T. Press, Cambridge (1966)
59. Wong, A.K., Kirby, G.C.: A hybrid numerical/experimental technique for determining the heat dissipated during low cycle fatigue. *Eng. Fract. Mech.* **37**, 493–504 (1990)